ELSEVIER

International Journal of Mass Spectrometry 199 (2000) 107–125

International Journal of Mass Spectrometry

Theoretical and experimental studies on the activation of ethylsilane by bare Co^+ cations

Susanne Bärsch, Thilo Böhme, Detlef Schröder, Helmut Schwarz*

Institut für Organische Chemie der Technischen Universität Berlin, Straße des 17. Juni 135, D-10623 Berlin, Germany

Received 6 July 1999; accepted 5 November 1999

Abstract

The potential-energy surface for the activation of ethylsilane by "naked" Co^+ ions is investigated by using density functional theory at the B3LYP level of theory and a valence double zeta basis. In particular, the pathways for the expulsion of the neutral molecules SiH_4, H_2, and CH_4 are examined, which are also observed in the mass spectrometric experiments. Five conceivable oxidative additions of the substrate to Co^+ are considered in the computational study, i.e. the primary insertions of the metal ion into the C–Si, C(1)–H, C(2)–H, C–C, and Si–H bonds. Comparison with experimental data shows qualitative agreement in that all experimentally observed products are predicted by theory to be formed in exothermic reactions with thermally surmountable barriers. Quantitatively, the ratio of the losses of SiH_4, H_2, and CH_4 is less well reproduced by the applied theoretical approach; however, the energetic differences between the rate determining transition states are too small to be resolved within the accuracy of most, if not all, nowadays theoretical methods applicable to transition-metal compounds. (Int J Mass Spectrom 199 (2000) 107–125) © 2000 Elsevier Science B.V.

Keywords: B3LYP; C–Si bond activation; H–Si bond activation; Ethylsilane; Co^+ cation

1. Introduction

The activation of C–H and C–C bonds by transition-metal complexes has been a matter of interest in chemistry for at least the last three decades both in solution [1–3] and in the gas phase [4–13]. However, as alkanes are chemically very inert substrates, their activation often requires the use of highly reactive reagents, such as coordinatively unsaturated transition metals. As a consequence, low selectivity is more the rule than the exception. There are at least two conceivable approaches aiming toward a more selective activation of C–H and C–C bonds. (1) The reactivity of the activating reagent, i.e. the transition metal, can be tuned by choice of appropriate ligands to favor activation of the bond of interest. (2) The use of functionalized substrates may induce more regioselective activations through the influence of the functional group. One example for the latter approach is, in analogy to Breslow's terminology [14–16], the so-called "remote functionalization" in the gas phase [17,18]. In short, remote functionalization involves initial coordination of the transition metal to the functionalized group ("docking"), followed by an internal solvation due to agostic interaction of the

* Corresponding author. E-mail: schw0531@www.chem.tu-berlin.de

Dedicated to Professor Henri Edouard Audier on the occasion of his 60th birthday.

PII S1387-3806(00)00172-X

metal ion with C–C and/or C–H bonds; thereby directing the transition metal toward a particular region of the aliphatic backbone of the substrate where eventually bond activation occurs.

Our group has studied the metal-ion mediated activation of several functionalized substrates in detail, e.g. nitriles, ketones, and alcohols, just to mention a few of them [17–25]. A particular case which has attracted much interest in our group lately, concerns the high selectivity observed in the remote functionalization of ω-silyl-substituted alkanenitriles [26,27]. To elucidate the underlying reaction mechanisms in more detail, combined experimental and theoretical studies on alkanenitriles [28] and an experimental study on the activation of alkylsilanes [29] were initiated. Further, as to the role of the metal ions' electronic structure, the activation of *n*-propyltrimethylsilane by Fe^+ and Co^+ reveals that the product branching ratio depends very much on the transition metal used [30]. However, despite use of extensive labeling, some questions remain unclear concerning the detailed mechanism of the metal-mediated bond activation, and theoretical studies were indicated. Albeit some significant progress, nowadays available theoretical methods can hardly be employed to answer these questions for open-shell systems of large size. In this context, even relatively small molecules such as *n*-propyltrimethylsilane are already too large a substrate to allow for a detailed and accurate theoretical treatment of the relevant potential-energy surfaces (PESs) at a sufficient level of theory.

As a first-order approximation, we have therefore decided to consider a smaller model system which allows both, theoretical and experimental investigations. In the present study, the reactivity of the system Co^+/ethylsilane is examined theoretically, inspired by mass spectrometric Fourier transform ion cyclotron resonance (FTICR) and sector-field mass spectrometry (MS) experiments. This study will be supplemented in the near future by a combined experimental and computational study of the Fe^+/ethylsilane system, which will then allow comparison of the electronic structure role in the activation behavior of these two important transition-metal ions [8,31–33].

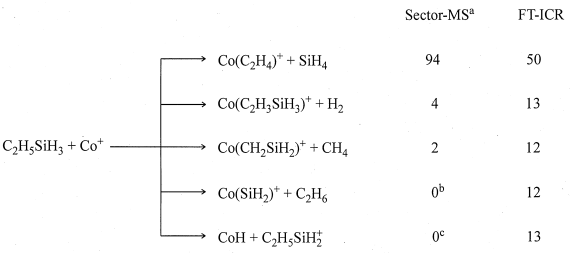

Fig. 1. Product distribution for Co^+/ethylsilane in FTICR and sector-MS experiments. The intensities are normalized to $\Sigma_{products} = 100\%$. Ion intensities <1% are omitted. (a) In addition, a small Co^+ peak (<1%) due to loss of the entire ligand is observed. (b) Although this product was not observed in the MI spectrum, a distinct peak at $m/z = 89$, corresponding to $Co(SiH_2)^+ + C_2H_6$ was found upon collisional activation. (c) This channel can be distinguished from the isobaric Co^+ fragmentation by isotopic labeling. Thus, for $Co^+/C_2H_5SiD_3$ only Co^+ is observed. Moreover, upon collisional activation also CoD but not CoH is lost from the labeled ion, supporting the assigned silylium structure.

2. Experiments

The Co^+/ethylsilane system is investigated by FTICR mass spectrometry [34,35] and metastable ion (MI) decay in a sector field mass spectrometer (sector-MS) [36–38]. These experimental techniques are chosen because they allow investigation of the system of choice under gas-phase conditions, i.e. free of any bulk effects; thereby permitting direct comparison with the theoretical data.

Both, sector-MS and FTICR show qualitative agreement in terms of prevailing losses of neutral SiH_4 from metastable $Co(C_2H_5SiH_3)^+$ and the $Co^+ + C_2H_5SiH_3$ couple, respectively. However, whereas loss of SiH_4 is the dominating channel in the sector-MS experiment with 94%, it accounts for only 50% of the products in FTICR. Further products observed in both experimental setups are the losses of H_2 and CH_4 (Fig. 1). In FTICR C_2H_6 and CoH are also formed. According to the product distributions and the nature of the products generated in the two experiments, MI studies with sector-field MS exhibit a higher selectivity than the FTICR experiments. We attribute this difference to a lower internal energy content of the metastable ions compared to the encounter complexes formed from the separated reac-

tants in the FTICR [39,40]. This conjecture is further supported by the appearance of a $Co(SiH_2)^+$ fragment due to loss of neutral C_2H_6, which is generated upon collisional activation (CA) in the sector-MS.

Labeling experiments using $Co^+/C_2H_5SiD_3$ are also performed in the sector-MS. The MI spectrum shows losses of SiD_3H (95%), CH_3D (2%), and D_2 (3%) [41]. Upon CA, also small amounts of HD and H_2 are produced, thus complicating the assignment of a definite mechanism for this reaction channel. However, the labeling experiments are quite helpful in that the formation of SiD_3H suggests involvement of the C–Si and a C–H bond, whereas the generation of CH_3D points to C–C and Si–D bond activation. Further, formation of D_2 clearly demonstrates initial Si–D insertion.

In addition, the reaction of $Co(C_2H_4)^+$ with silane is considered under FTICR conditions, but no product formation at a reasonable rate constant is observed ($k < 2 \times 10^{-12}$ cm^3 molecule^{-1} s^{-1}), suggesting that $D_0[Co(SiH_4)^+] < D_0[Co(C_2H_4)^+] = 44.5 \pm 2.1$ kcal/mol [42].

3. Theoretical methods

In the calculations, the program package GAUSSIAN94 is employed [43]. The relatively large size of the systems explored requires the use of the CRAY-YMP supercomputer at the Konrad-Zuse-Zentrum für Informationstechnik Berlin in terms of both, memory supply and computer time. Density functional theory (DFT) at the B3LYP level of theory [44,45] is utilized because it has been shown to provide reasonably accurate energetics for transition-metal mediated activation of organic substrates [28,46–48]. A valence double-zeta (VDZ) quality basis set as developed by Ahlrichs and co-workers [49] is used for Co, H, C, and Si; it is denoted BS1 and consists of the following basis functions and contractions: H (4*s*)/[2*s*], C (7*s*4*p*)/[3*s*2*p*], Si (10*s*7*p*)/[4*s*3*p*], and Co (14*s*8*p*5*d*)/[5*s*2*p*2*d*].

All structures discussed correspond to fully optimized stationary points for which both, the gradients as well as the displacements from analytical second derivatives fulfill the standard convergence criteria [50]. All stationary points are characterized by frequency analysis. In addition, the transition structures (TSs) are verified by intrinsic reaction coordinate (IRC) [51,52] calculations, which connect the TSs with the corresponding minima. For the sake of computer time, the IRC calculations are interrupted when structural proximity to the related minima is reached, rather than completely exploring the conformational space. All energies are corrected for the zero-point vibrational energy (ZPVE) contributions and, unless noted otherwise, refer to 0 K.

Even small basis sets usually yield reliable results in the geometry optimizations, whereas the energetics of the system may depend more on the size of the basis set. To test this very general assumption, the effect of a larger basis including polarization functions (BS2) in our B3LYP calculations is evaluated. Some trial geometry optimizations are performed on the species $CoC_2H_4^+$, $CoSiH_4^+$, TS**11/12**, and $C_2H_5SiH_3$. The BS2 basis set is of approximately valence triple zeta (VTZ) quality, and consists of the Wachters+*f* basis for cobalt [53–55] and the cc-pVTZ basis according to Dunning and co-workers [56–58] for Si, C, and H. The contractions for the basis set read as follows: H (7*s*2*p*1*d*)/[3*s*2*p*1*d*], C (12*s*7*p*2*d*1*f*)/[4*s*3*p*2*d*1*f*], Si (15*s*9*p*2*d*1*f*)/[5*s*4*p*2*d*1*f*], and Co (14*s*11*p*6*d*3*f*)/[8*s*6*p*4*d*1*f*]. Single-point energy calculations on the critical parts of the PES are also performed using the B3LYP/BS2 approach, where we define the transition states of the rearrangement, the entrance channel, and the exit channels as the critical species along all reaction paths.

4. Results

The PES for the activation of ethylsilane **1** by "naked" Co^+ cations is calculated for five conceivable activation mechanisms, i.e. the initial insertions of the Co^+ ion into the C–Si, C(2)–H, C(1)–H, C–C, or Si–H bonds (Fig. 2).

The geometry calculations presented here are performed by using the B3LYP/BS1 approach. Some trial geometry optimizations using B3LYP and the

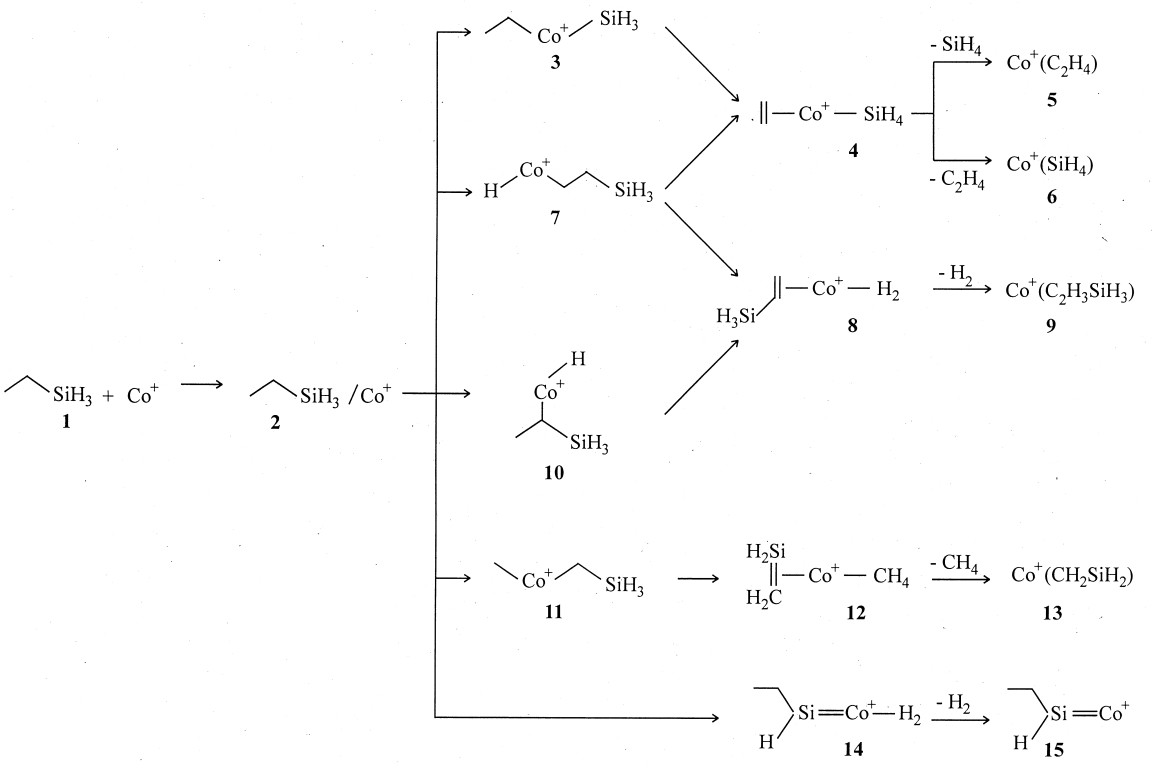

Fig. 2. Schematic description of the five calculated reaction pathways of the Co^+/ethylsilane system. Note, that only the expected minima along the reaction coordinate are displayed. Transition states connecting the respective minima are discussed in the text.

BS2 basis set are performed to make sure that the small basis is efficient enough to yield reliable geometric features. These calculations involve the species $CoC_2H_4^+$, $CoSiH_4^+$, TS**11/12**, and $C_2H_5SiH_3$. The BS2 optimized geometries agree very well with the BS1 optimized geometries with deviations in the bond lengths between the two methods below 0.03 Å, such that we conclude that the B3LYP/BS1 approach is sufficient for the geometry optimizations. Only the triplet surface is considered for several reasons. (1) The experimentally determined, well established triplet–quintet splitting of Co^+ ($^3F \rightarrow {}^5F$) amounts to 8.3 kcal/mol [59], whereas the corresponding triplet–singlet splitting is even more pronounced. (2) Vanquickenborne and co-workers found the quintet surface to be of little importance for the activation of methane by Co^+ [60]. (3) Exploratory calculations on the quintet and singlet surfaces reveal a very strong preference of the Co^+ system toward a triplet spin state, as is illustrated by the following examples. For instance, the fully optimized structures for the encounter complexes on the singlet and quintet surfaces are located 16.1 and 19.1 kcal/mol, respectively, above the most stable conformer of the encounter complex on the triplet surface. In addition, the primary product of C–Si bond insertion (see the following) is also examined for all three spin states. Here, the singlet structure is 17.2 kcal/mol and the quintet structure is 20.0 kcal/mol higher in energy than the corresponding triplet species. Consequently, the singlet and quintet surfaces are unlikely to participate in the reaction, and we assume that consideration of the triplet PES provides a sufficient description of the reactivity of the system.

Because of the known deficiency of B3LYP to treat atoms accurately [61–64], we expect that the

theoretically predicted complexation energy of Co^+ and **1** is somewhat too large. Thus, the entrance channel is likely to be associated with a larger error than the remaining parts of the PES to which we attribute an average error of ±8 kcal/mol. This uncertainty is based on the average deviations of some calculated bond-dissociation energies and heats of formation for model processes with known literature values [65] as well as comparison with B3LYP investigations of transition metal/hydrocarbon systems with basis sets of similar quality [66–68].

In the following, we first describe the reactants and the encounter complex because they are common to all five insertion pathways. Then the remaining minima and transition states of the five individual routes are discussed separately in the order of their appearance in Fig. 2.

In agreement with the established electronic states [59], the ground state of Co^+ is calculated to be ^3F. The corresponding quintet excited state is calculated to be only 2.5 kcal/mol above the ground state compared to the experimental value of 8.3 kcal/mol [59]. The deviation from the experimental state splitting highlights the known problem associated with the B3LYP approach in the calculation of atoms as mentioned previously [61]. The optimized minimum structure of ethylsilane **1** ($^1A'$) has C_s symmetry and is displayed in Fig. 3. Note that throughout the article we refer to the two different carbon atoms as C(1) and C(2), according to IUPAC nomenclature. The lengths of the Si–C, C–H, C–C, and Si–H bonds of **1** are further used as internal references for typical single bonds between these elements.

The η^4-coordinated encounter complex **2** is the most stable conformer localized, and set to E_{rel} = 0.0 kcal/mol on the energy scale. In **2**, the Co^+ cation interacts with C(2), silicon, and two hydrogen atoms one from C(2) and the other from silicon, respectively; these hydrogen atoms are directed towards Co^+ in an agostic fashion [69,70]. The Co–Si distance of 2.77 Å (as compared to r_{CoSi} = 2.44 Å in **3**) indicates an electrostatic interaction, whereas the Co–C interaction is much weaker as displayed by the long Co–C distance of 2.50 Å (r_{CoC} = 1.94 Å in **3**). The two hydrogen atoms approaching Co^+ show Co–H bond lengths of r_{CoH} = 1.85 and 1.67 Å, whereas the corresponding C–H and Si–H bonds are elongated by 0.03 and 0.12 Å as compared to the one of free ethylsilane; this again indicates a by and large electrostatic interaction.

Three other conformers of the encounter complex **2** are localized during the calculations, all of which are less stable than **2**; for the sake of clarity, these conformers are not included in Fig. 3. Briefly, a η^3-coordinated conformer is located only 0.8 kcal/mol above **2**. Here, interaction occurs between Co^+ and the silicon atom as well as two of the silylic hydrogen atoms. Another conformer (E_{rel} = 4.1 kcal/mol) shows strong interactions between the silicon and Co^+ (r_{SiCo} = 2.50 Å) as well as C(1) and Co^+ ($r_{CoC(1)}$ = 2.45 Å). Finally, another η^3 complex (E_{rel} = 8.9 kcal/mol) is characterized by the interaction of Co^+ with C(1) ($r_{CoC(1)}$ = 2.10 Å) and both hydrogen atoms on C(1) (r_{CoH} = 1.94 Å); in this conformer no interaction with silicon is achieved. The fact that the silicon-bound conformers are at least 4.8 kcal/mol more stable than the carbon-only bound conformer indicates that coordination to the silyl-group is notably stronger than that to the alkyl moiety. Note that in the construction of the PESs only the most stable conformers are considered, because we assume the barriers for the interconversion of the different conformers to be much lower than the barriers for cleavage and/or formation of covalent bonds.

4.1. C–Si bond insertion

From the encounter complex **2**, the reaction commences via TS**2/3** toward **3** (Fig. 4). In TS**2/3** (E_{rel} = 12.5 kcal/mol), the cobalt ion approaches the C–Si bond, which is elongated to 2.72 Å. The C_1-symmetric structure exhibits a single imaginary frequency ($i240.8\ cm^{-1}$) which corresponds to the stretch of the C–Si bond together with a widening of the C(1)–Co–Si angle.

The most stable conformer of the C–Si insertion complex **3** (E_{rel} = 9.2 kcal/mol) exhibits an eclipsed conformation with a dihedral angle [Si–Co–C(1)–C(2)] of 105° and Co–C(1) and Co–Si bond lengths of

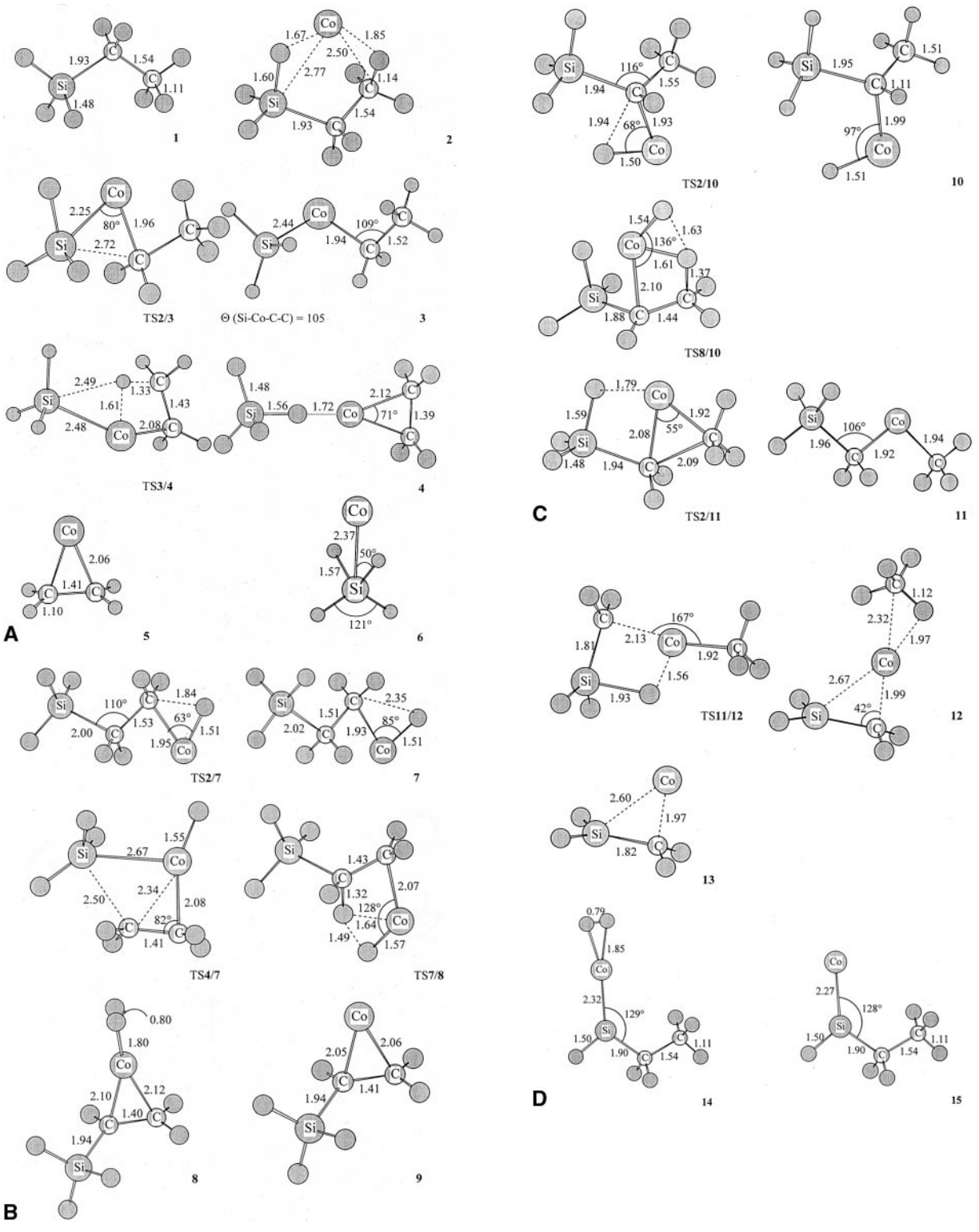

Fig. 3. Minima and transition structures of the Co^+/ethylsilane system calculated at the B3LYP/BS1 level of theory. Bond lengths are given in angstroms and angles in degrees.

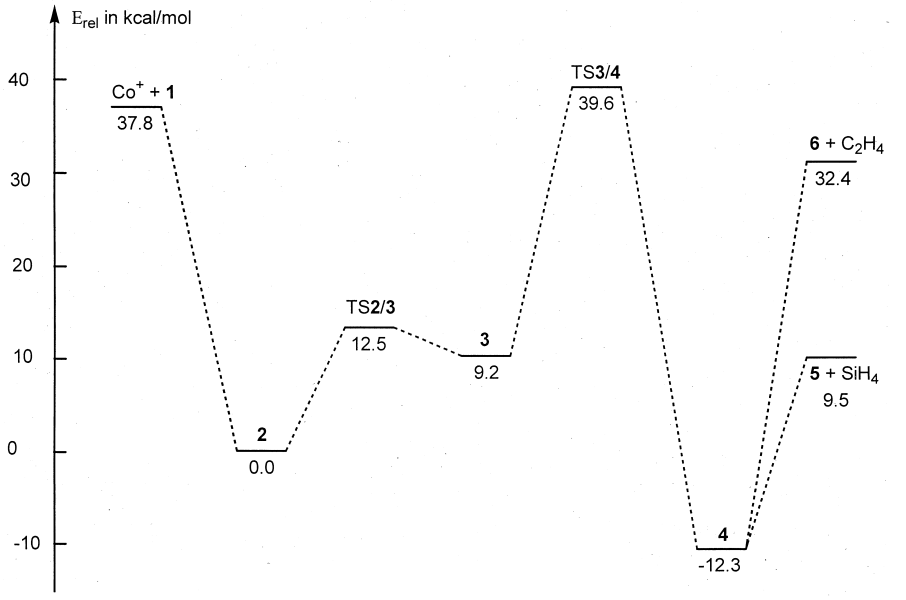

Fig. 4. B3LYP/BS1 PES of the C–Si insertion pathway of $Co^+ + C_2H_5SiH_3$ relative to the lowest-lying encounter complex **2**; ZPVE corrections are included, and the relative energies are given in kilocalories per mole.

$r_{CoC(1)} = 1.94$ and $r_{CoSi} = 2.44$ Å. At least two other rotamers (not shown) exist for the C–Si inserted structure. The first one is located only 0.1 kcal/mol above **3**, showing an eclipsed conformation with a dihedral angle [Si–Co–C(1)–C(2)] of 150°. The second structure ($E_{rel} = 10.4$ kcal/mol) has a gauche conformation with a dihedral angle [Si–Co–C(1)–C(2)] of only 52°, thus causing a repulsive interaction between methyl and silyl groups.

From **3**, the reaction proceeds toward TS**3/4** ($E_{rel} = 39.6$ kcal/mol). The geometrical features of the transition structure describe a concerted process of (1) C–H bond cleavage at the methyl group (β-hydrogen transfer, $r_{CH} = 1.33$ Å) and (2) transient formation of a Co–H bond ($r_{CoH} = 1.61$ Å). The imaginary frequency ($i1184$ cm^{-1}) of the multicentered [66] TS corresponds to the migration of the hydrogen from cobalt towards the silyl group, along with some rearrangement in the C_2H_4 moiety. Note, however, that in the TS the Co–C bonds are distinctly different ($r_{CoC(2)} = 2.22$ versus $r_{CoC(1)} = 2.08$ Å) such that the η^2 coordination of the ethylene ligand is not yet achieved.

Complex **4**, $Co(C_2H_4)(SiH_4)^+$, is formed after passing TS**3/4** and corresponds to the most stable structure along the C–Si bond insertion PES. In **4** ($E_{rel} = -12.3$ kcal/mol), the ethylene molecule is attached to one side of the Co^+ atom whereas the SiH_4 molecule is located on the opposite side with one hydrogen atom pointing directly from silicon toward Co^+, forming a Co–H–Si angle of 180°. Thus, SiH_4 is connected to the metal ion only by a weak electrostatic $Co \cdots H \cdots SiH_3$ interaction, whereas ethylene is η^2 coordinated to the cobalt cation; the latter is indicated by two identical Co–C bonds of $r_{CoC} = 2.12$ Å and a C–C bond with a bond length of $r_{CC} = 1.39$ Å, typical for a C–C double bond. In another conformer ($E_{rel} = -9.3$ kcal/mol, not shown), the SiH_4 moiety is bound such that the silicon atom electrostatically interacts with Co^+, with the silicon–cobalt axis intersecting the angle of two of the hydrogen atoms whereas the bonding to the C_2H_4 moiety is alike in both conformers, as displayed by identical geometries of the $Co(C_2H_4)^+$ substructures.

From **4**, the product channels $Co(C_2H_4)^+ + SiH_4$ ($E_{rel} = 9.5$ kcal/mol) and $Co(SiH_4)^+ + C_2H_4$

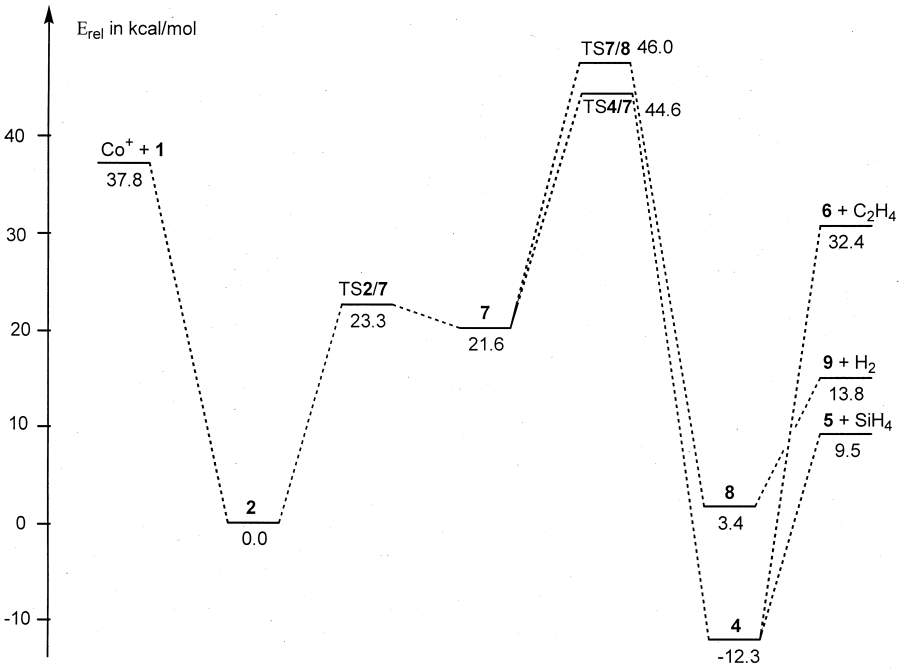

Fig. 5. B3LYP/BS1 PES of the C(2)–H insertion pathway of $Co^+ + C_2H_5SiH_3$ relative to the lowest-lying encounter complex **2**; ZPVE corrections are included, and the relative energies are given in kilocalories per mole.

(E_{rel} = 32.4 kcal/mol) can be reached by simple dissociation (Fig. 4). Due to the calculated higher stability of $Co(C_2H_4)^+$ (D_0 = 50.6 kcal/mol) as compared to $Co(SiH_4)^+$ (D_0 = 27.7 kcal/mol), loss of silane from **4** is favored by 22.9 kcal/mol compared to elimination of ethylene. The cobalt–ethylene complex **5** exhibits a $^3A_2$ ground state in C_{2v} symmetry. The bond length of the C–C bond (r_{CC}) of 1.41 Å is slightly elongated as compared to free ethylene (r_{CC} = 1.34 Å) in accord with bond formation between Co^+ and ethylene and concomitant weakening of the C–C double bond. The calculated bond dissociation energy of $D_0[Co(C_2H_4)^+]$ = 50.6 kcal/mol, however, has to be viewed with care, because (1) the error associated with the calculation of the metal cation is rather large as mentioned previously [61], and (2) the bond dissociation energy of this complex is experimentally determined to be 44.5 ± 2.1 kcal/mol [42]. However, the qualitative view appears to be correct, e.g. the $Co(C_2H_4)^+$ complex is more strongly bound than $Co(SiH_4)^+$ which is consistent with the absence of ethylene loss in the experiment. Note that neutral SiH_4 has been calculated in C_s symmetry with an $^1A'$ ground state, because the optimized structure shows slight deviations from tetrahedral symmetry. Attempts to optimize the structure in tetrahedral symmetry resulted in small imaginary modes during frequency analysis. In the $Co(SiH_4)^+$ complex **6**, the cobalt–silicon axis intersects the angle between two of the hydrogen atoms on silicon, forming Co–Si–H angles of 50°. The distance of r_{CoSi} = 2.37 Å points to a covalent bond with a bond length comparable to the cobalt-silicon distance in the insertion product **3**.

4.2. C–H bond insertion

Owing to its relationship to the C–Si insertion path (Fig. 2), activation of the C(2)–H bond is considered first. Starting from the encounter complex **2**, initial insertion into the C(2)–H bond yields **7** via TS**2/7** (E_{rel} = 23.3 kcal/mol, Fig. 5). This TS shows a product-like structure, the major structural difference between TS**2/7** and **7** concerns the length of the C–H

bond into which the cobalt cation inserts (r_{CH} = 1.11 Å in **2**, r_{CH} = 1.84 Å in TS**2/7**, and r_{CH} = 2.35 Å in **7**). The imaginary frequency (i550 cm^{-1}) corresponds to a large extent to the motion of the hydrogen atom away from C(2), thus increasing the (C–Co–H) angle from 63° in the TS to 85° in **7**. In addition, the movement of C(2) toward C(1) accompanied with a slight shortening of the C–C bond (from 1.53 Å in TS**2/7** to 1.51 Å in **7**) contributes to the transition mode.

For the C(2)–H insertion structure three conformers are localized. The most stable species **7** (E_{rel} = 21.6 kcal/mol) corresponds to an anti-conformer with respect to the C–C bond. Two other conformers (not shown) are located at E_{rel} = 26.4 kcal/mol and E_{rel} = 30.3 kcal/mol, respectively. The former corresponds to an anti-conformer, with a different Co–C(2) bond length and C(2)–Co–H angle as compared to **7** [$r_{CoC(2)}$ = 1.99 Å and C(2)–Co–H = 102° versus $r_{CoC(2)}$ = 1.93 Å and C(2)–Co–H = 85° in **7**]. These slight geometric deviations of the two conformers are unlikely to account for an energetic difference of 4.8 kcal/mol between **7** and the corresponding conformer at E_{rel} = 26.4 kcal/mol; thus rather pointing to a different electronic structure of the latter. This conjecture is further supported by the natural bond order (NBO) analysis of the two species, which shows different bonding orbitals for the two species in the insertion region. The third conformer exhibits similar bond lengths as the conformer at 26.4 kcal/mol; in addition, the silyl group and the CoH unit are arranged in a gauche conformation with respect to the C–C bond [dihedral angle Si–C(1)–C(2)–Co = 45°]. Therefore, it is readily understood that this conformer is disfavored by 8.7 kcal/mol compared to **7**, probably due to a joint action of electronic structure and conformational disadvantage. From **7**, the reaction may continue via two different pathways, either β-SiH_3 or β-H migration. First, the β-SiH_3 migration pathway is considered. The transition from **7** to **4** proceeds via TS**4/7** (E_{rel} = 44.6 kcal/mol). Starting from **7**, rotation of the C–C bond and movement of the hydrogen atom on Co^+ toward the SiH_3 group leads to TS**4/7**. Both motions contribute to the imaginary frequency of i475 cm^{-1}. In the TS the C–Si bond is broken (r_{SiC} = 2.50 Å), and formation of the ethylene ligand is in progress as is apparent from (1) the change in the bond lengths of the two different Co–C bonds (**7**: $r_{CoC(1)}$ = 2.36 Å and $r_{CoC(2)}$ = 1.93 Å; TS: $r_{CoC(1)}$ = 2.34 Å and $r_{CoC(2)}$ = 2.08 Å), and (2) the planarization of the C_2H_4 moiety [dihedral angle H–C(1)–C(2)–H amounts to 46° in **7** and only 0.3° in **4**], going along with a change of hybridization from sp^3 in **7** to sp^2 in **4** as already discussed. Structure **4** can account for the losses of neutral silane and ethylene, respectively, resulting in the formation of product complexes **5** and **6**.

Next, the pathway for the β-H migration is investigated. Starting from **7**, the product complex **8** is reached via TS**7/8** (E_{rel} = 46.0 kcal/mol) which involves a rotation of the Co–C(2) bond [angle C(2)–Co–H = 85° versus 128° in **7** and TS**7/8**, respectively] concomitant with elongation of a C(1)–H bond assisted by an additional Co–H interaction in the TS ($r_{C(1)H}$ = 1.32 Å and r_{CoH} = 1.64 Å). The imaginary frequency of TS**7/8** (i972 cm^{-1}) corresponds to a motion of both hydrogen atoms on the cobalt atom approaching each other. The reaction continues toward **8** (E_{rel} = 3.4 kcal/mol), which consists of an intact H_2 molecule (r_{HH} = 0.80 Å), electrostatically interacting with the cobalt atom (r_{CoH} = 1.80 Å) and a vinylsilane moiety. Similar to previous examples [66–68], no indications for the existence of a dihydrido minimum are found; instead the reaction directly proceeds from **7** to **8** via the multicentered TS**7/8**. The C–C double bond (r_{CC} = 1.40 Å) of the vinylsilane ligand binds in a π-type manner to the cobalt cation. The Co–C bond lengths of $r_{CoC(1)}$ = 2.10 Å and $r_{CoC(2)}$ = 2.12 Å differ slightly, but are comparable to the corresponding r_{CoC} of the cobalt ethylene complex **5** (r_{CoC} = 2.06 Å) and to the Co–C bond length in **4**, r_{CoC} = 2.12 Å. From **8**, the reaction continues further to the dehydrogenation product **9**, $Co(C_2H_3SiH_3)^+$, by loss of neutral H_2 (E_{rel} = 13.8 kcal/mol). In **9**, the cobalt atom is located above the C–C bond (r_{CC} = 1.41 Å) with Co–C bond lengths of $r_{CoC(1)}$ = 2.05 Å and $r_{CoC(2)}$ = 2.06 Å. This indicates an almost symmetric π interaction between the C–C double bond and the cobalt cation. The influence of the silyl moiety seems to be rather small, in

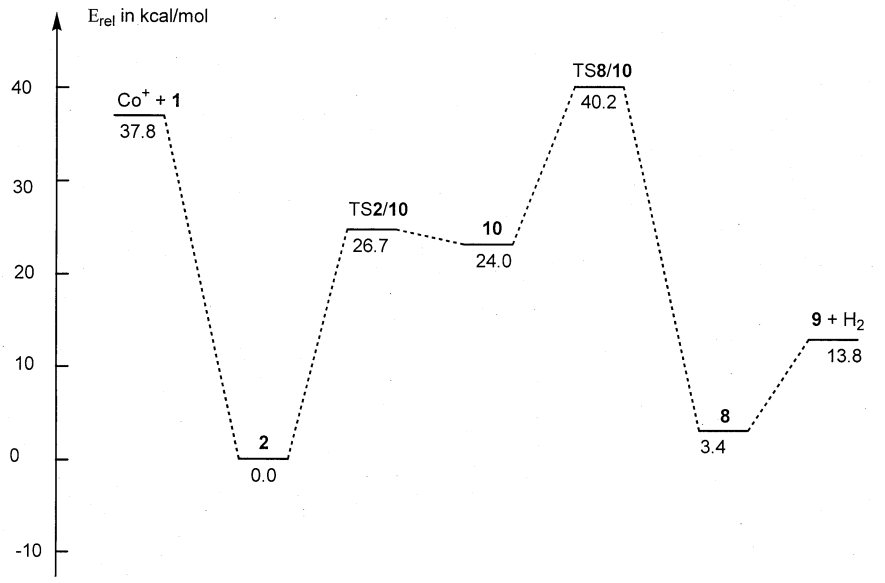

Fig. 6. B3LYP/BS1 PES of the C(1)–H insertion pathway of $Co^+ + C_2H_5SiH_3$ relative to the lowest-lying encounter complex **2**; ZPVE corrections are included, and the relative energies are given in kilocalories per mole.

analogy to **8**, as both Co–C bonds exhibit approximately the same bond lengths. The Mulliken population analysis predicts the positive charge almost entirely on Co^+ ($q_{Co^+} = +0.96$); hence charge transfer is negligible.

C(1)–H bond insertion (Fig. 6) commences from the encounter complex via TS**2/10** (E_{rel} = 26.7 kcal/mol). Thus, the C(1)–H bond elongates from r_{CH} = 1.11 Å in **2** to r_{CH} = 1.94 Å in TS**2/10**, whereas Co–H and Co–C bonds are preformed (r_{CoH} = 1.50 Å and $r_{CoC(1)}$ = 1.93 Å). TS**2/10** is very much product-like, and the imaginary frequency of *i*407 cm^{-1} mainly corresponds to a movement of a hydrogen away from C(1), thus opening the C(1)–Co–H angle from 68° in the TS to 97° in **10**, along with some coupling of rotational motions of the methyl and silyl groups. The C_1 symmetric insertion structure **10** (E_{rel} = 24.0 kcal/mol) exhibits bond lengths of $r_{CoC(1)}$ = 1.99 Å and r_{CoH} = 1.51 Å. Following the reaction path, TS**8/10** is localized at E_{rel} = 40.2 kcal/mol. The C(1)–Co–H angle in TS**8/10** is widened (from 97° in **10** to 136° in the TS) and one C(2)–H bond of the methyl group is elongated ($r_{C(2)H}$ = 1.37 Å) with the hydrogen atom moved toward the metal; thus a Co–H bond is formed (r_{CoH} = 1.61 Å). The H–H distance of r_{HH} = 1.63 Å is far from formation of a dihydrogen molecule. This points to an early TS on the reaction coordinate, in agreement with the structural similarity between TS**8/10** and **10**. Two major motions contribute to the imaginary frequency of *i*810 cm^{-1}, i.e. the approach of the two hydrogen atoms towards each other and planarization of the two remaining hydrogen atoms on C(2). After traversing TS**8/10**, structure **8** is reached, which then may dissociate into product complex **9** and H_2. As these parts of the PES are common between the C(1)–H insertion and the C(2)–H insertion discussed above, they need not to be discussed further.

4.3. C–C bond insertion

Starting from the encounter complex **2**, C–C bond activation involves TS**2/11** (E_{rel} = 19.8 kcal/mol) en route to the insertion structure **11** (Fig. 7). In the TS the C–C bond is elongated from r_{CC} = 1.54 Å in **2** to r_{CC} = 2.09 Å in the TS. The Co–C(2) distance decreases to 1.92 Å in TS**2/11** indicating an increased Co–C(2) interaction. The imaginary frequency (*i*305

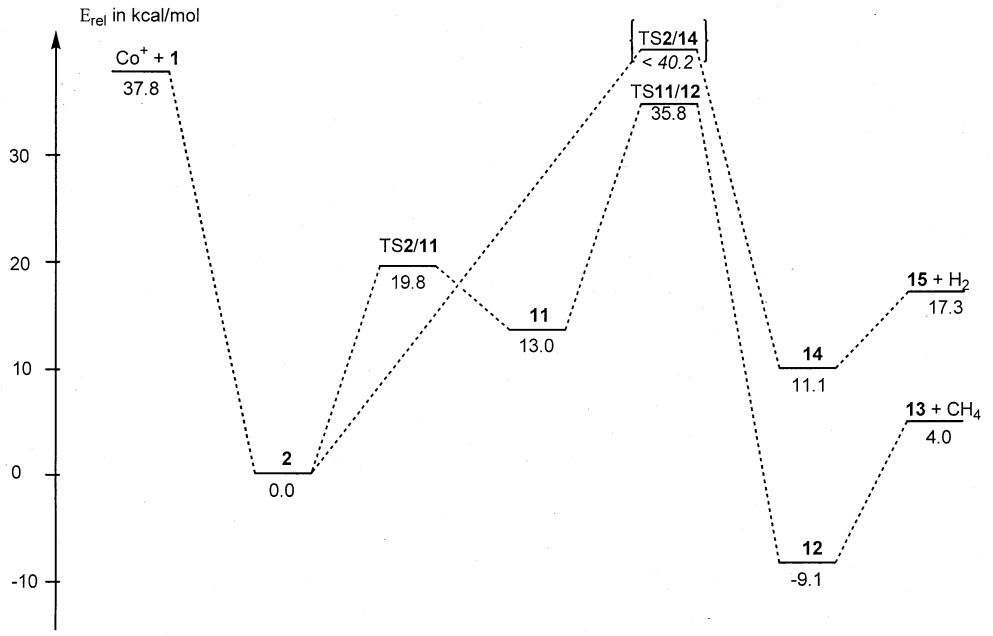

Fig. 7. B3LYP/BS1 PES of the C–C and Si–H insertion pathway of $Co^+ + C_2H_5SiH_3$ relative to the lowest-lying encounter complex **2**; ZPVE corrections are included, and the relative energies are given in kilocalories per mole. The energetic location of TS**2/14** (in parentheses) is obtained from a comparison of experimental and theoretical results, see text.

cm^{-1}) corresponds to an elongation of the C–C bond and subsequent insertion of the cobalt cation into the C–C bond. The insertion minimum **11** (E_{rel} = 13.0 kcal/mol) exhibits two almost equivalent Co–C bonds with r_{CoC} = 1.92 and 1.94 Å, respectively. The molecule shows an anti-conformation with respect to the Co–C(1) bond.

From **11**, the product complex **12** can be reached, which serves as a precursor for loss of methane. Interestingly, C–C bond activation via TS**11/12** has the lowest energy barrier (E_{rel} = 35.8 kcal/mol) of all activation pathways considered here for a β-bond activation. The motion of one hydrogen atom away from the silyl toward the methyl group is displayed by the elongated Si–H distance of the migrating hydrogen atom as compared to the two hydrogen atoms remaining on the silicon atom (r_{SiH} = 1.93 versus 1.48 Å). The TS can therefore be regarded as a cobalt cation, surrounded by three ligands, i.e. H, CH_3, and CH_2SiH_2. The angle between the two carbon atoms is 167°, such that the methyl moiety and CH_2SiH_2 are located on almost exactly opposite sides of the cobalt atom, thereby minimizing steric hindrance. The imaginary frequency of i578 cm^{-1} corresponds to the motion of the hydrogen atom away from the silyl and toward the methyl group with minor contributions from the rotation of the two remaining hydrogen atoms on silicon.

Structure **12** (E_{rel} = −9.1 kcal/mol) consists of a CH_4 molecule weakly interacting with the metal and a silaethene ligand attached to the opposite side of the Co^+. The structure of the CH_4 subunit is slightly perturbed from tetrahedral symmetry because of the η^2 coordination of the ligand via two hydrogen atoms to Co^+. This interaction causes an elongation of the coordinated C–H bonds as compared to the C–H bonds pointing away from Co^+ (r_{CH} = 1.12 versus 1.10 Å). The silaethene moiety is side-on coordinated to Co^+ with r_{CoC} = 1.99 Å and r_{CoSi} = 2.67 Å. **12** serves as a direct precursor for loss of methane concomitant with formation of $Co(CH_2SiH_2)^+$, **13**. Interestingly, this exit channel is predicted as the lowest in energy demand of all product channels (E_{rel} = 4.0 kcal/mol). This observation is in agree-

ment with the calculated reaction enthalpy of 15.5 kcal/mol for the ligand exchange reaction $Co(CH_2SiH_2)^+ + C_2H_4 \rightarrow Co(C_2H_4)^+ + CH_2SiH_2$. The increased stability of $Co(CH_2SiH_2)^+$ is not only rationalized by the higher polarizability of the CH_2SiH_2 ligand compared to C_2H_4, but also points to the involvement of mesomeric species, i.e. $Co^+–CH_2–SiH_2 \leftrightarrow Co–CH_2–SiH_2^+$. The latter is supported by the Mulliken population analysis ($q_{Co^+} = +0.86$, $q_{Si} = +0.57$, $q_C = -0.43$). In addition, structural features of **13** assist this conjecture as well; the Co–C bond length of $r_{CoC} = 1.97$ Å is shorter than the corresponding Co–C bond length in the above described olefin complexes, whereas the Co–Si distance of $r_{CoSi} = 2.60$ Å is relatively long. This situation coincides with an asymmetric side-on coordination already discussed for **12**.

4.4. Si–H bond insertion

This mechanism seems to proceed in a different manner compared to the other insertion reactions described above (Fig. 7). The pathway of insertion into one Si–H bond, which we expected first, could not be confirmed. Moreover, not even an intermediate Si–H inserted structure could be located; any of the numerous input structures used in the geometry optimizations either converged to encounter complex **2** or product structure **14**. Therefore, we suggest that a genuine Si–H inserted structure does not exist as a stationary point at the level of theory employed; instead the reaction proceeds via a four-centered transition state directly from **2** to **14**, $(H_2)Co(SiHC_2H_5)^+$. To the best of our knowledge, no calculations on the activation of silane by M^+ exist to corroborate this type of mechanism [71,72]. However, the insertion into two Si–H bonds would be in accord with quantum-chemical calculations of Morokuma and co-workers [73–75], who investigated the reaction of late transition metals with CH_4. They were unable to locate a species corresponding to $H–M–CH_3^+$, but found that the reaction proceeds directly from $M(CH_4)^+$ to $(H_2)MCH_2^+$ for M = Co, Fe. However, in the system studied here, all attempts failed so far to locate the corresponding multicentered TS**2**/**14**. Our search for TS**2**/**14** included various plausible input structures as well as the linear synchronous transit [76], QST2, and QST3 optimization methods [77] implemented in GAUSSIAN94. However, in analogy to the results of Morokuma et al. [73–75] discussed previously, we assume that **2** and **14** are connected by a single TS.

Minimum **14** ($E_{rel} = 11.1$ kcal/mol) is localized and characterized as a cobalt cation interacting with two ligands, i.e. a slightly distorted hydrogen molecule and an ethylsilylidene unit; **14** thus serves as a precursor for loss of H_2 to afford **15** ($E_{rel} = 17.3$ kcal/mol). The Co–Si bond lengths of $r_{CoSi} = 2.32$ Å and 2.27 Å in **14** and **15** are considerably shorter than the C–Si bond in **3** ($r_{CoSi} = 2.44$ Å). This kind of bond shortening is in line with formal cobalt–silicon double bonds in the silylidene complexes in **14** and **15**. The structure of the free cobalt silylidene **15** closely resembles the geometry of **14**. This is readily explained, because loss of the electrostatically bound H_2 ligand from **14** does not induce changes in the electronic and geometric structure of the silylidene unit.

5. Discussion

Some more general features of the above described reaction paths need to be outlined first. (1) The calculated minima and transition structures of the C–Si, C(1)–H, and C–C insertion paths are lower in energy or in close vicinity of the entrance channel. These reactions are therefore expected to occur under thermal conditions, which is in agreement with the experimentally observed findings. The C(2)–H insertion pathway is also approximately thermoneutral within the error margin of the method of 8 kcal/mol. However, the predicted barriers of more than 7 kcal/mol above the entrance channel, compared to the existing energetically less demanding pathways, render the C(2)–H insertion rather unlikely to occur at thermal energies. Therefore we exclude the C(2)–H insertion from our further considerations. An addi-

tional hint supporting this argument comes from recent Rice-Ramsperger-Kassel-Marcus (RRKM) calculations [78–80]. Here, the B3LYP potential energy surface is calculated first for the reactions of Ni^+ with propane and *n*-butane and used as basis for the following RRKM calculations. The RRKM treatment yields the result, that all the B3LYP transition states in the stationary calculations are calculated too high and have to be shifted to lower energies. The correction is thus applied in the same direction for all transition states. If this is applied to our system, the C(2)–H insertion is assumed to shift to lower energies; but as the other dehydrogenation pathways are likely to shift into the same direction, the lower energy dehydrogenation pathways are presumably the preferred reaction pathways. The activation of the Si–H bond is clearly exothermic from a thermochemical point of view, because all minima are located well below the entrance channel. As we did not manage to locate TS**2/14**, the barrier associated with this rearrangement remains uncertain. However, the pronounced loss of D_2 from the labeled substrate $C_2H_5SiD_3$ demands the inclusion of this pathway in the discussion. (2) In general, the TSs of the initial oxidative additions are less energy demanding than the barriers associated with the further rearrangements and reductive elimination en route to the product complexes. Hence, the latter are rate determining for the Co^+/ethylsilane system; in contrast, initial bond insertion can be considered as facile and not rate determining. This finding is in accord with previous calculations on the activation of organic substrates by late transition-metal cations [66–68]. The following discussion therefore concentrates on the rate-determining TSs and the calculated thermochemistry of the products.

5.1. Loss of silane

Elimination of silane is conceivable either via primary insertion in the C–Si bond (Fig. 4) or via primary C(2)–H bond activation (Fig. 5). On the C–Si insertion surface (Fig. 4), the relevant TS is TS**3/4** at E_{rel} = 39.6 kcal/mol compared to the entrance channel at E_{rel} = 37.8 kcal/mol. Once this barrier is surmounted, **4** is formed and has enough internal energy to directly decompose into the products $Co(C_2H_4)^+$ and SiH_4 as well as $Co(SiH_4)^+$ and neutral ethylene. Due to the strong Co^+–ethylene bond, elimination of SiH_4 is thermochemically preferred over that of C_2H_4. However, comparison with literature data shows an overestimation of the $Co(C_2H_4)^+$ bond dissociation energy by 5.9 kcal/mol [42]. To the best of our knowledge, no data on the bond dissociation energy of $Co(SiH_4)^+$ are available in the literature. Notwithstanding, a change in the overall picture is not expected, even when these two exit channels may in reality be closer in energy than predicted in the calculations.

A second conceivable pathway for formation of **4** proceeds via initial C(2)–H insertion and consecutive reaction via TS**4/7** (Fig. 5). Both pathways are strongly exothermic; however, whereas the C–Si insertion pathway remains below the entrance channel, the C(2)–H insertion pathway involves a barrier located 6.8 kcal/mol above separated Co^+ and $C_2H_5SiH_3$. Although the distinction is not unambiguous, because of the error bars of the calculations, initial activation of the C–Si bond is proposed as the energetically least demanding path for the formation of **4**.

5.2. Dehydrogenation

Elimination of molecular hydrogen may occur via two entirely different reaction pathways involving isomeric product species, i.e. the silene **9** and the silylidene **15**. Both types of species have been generated before, in the gas phase [81–83] as well as in solution [84–92].

Two possible pathways [primary C(1)–H or C(2)–H insertions as depicted in Figs. 5 and 6, respectively] lead to formation of **8**, the precursor of the silene complex **9**. TS**8/10** of the C(1)–H insertion pathway is located at E_{rel} = 40.2 kcal/mol, thus only 2.4 kcal/mol above the entrance channel. After traversing TS**8/10**, formation of **8** and subsequent loss of H_2 is easily accomplished and not associated with any further energy demand. On the C(2)–H insertion PES, however, the pathway for formation of **8** proceeds via

TS**7/8** at E_{rel} = 46.0 kcal/mol. Accordingly, the C(1)–H insertion pathway may be preferred for thermalized ions, while the route involving initial activation of the C(2)–H bond may require elevated energies. Thus, formation of **9** is expected to proceed via the C(1)–H insertion pathway.

Dehydrogenation may also lead to the isomeric product **15** (Fig. 7). However, as we could not locate TS**2/14**, a direct comparison to the route leading to **9** is impossible. Thermochemically, formation of **15** is disfavored by 3.5 kcal/mol compared to **9**. Nevertheless, the experimental data obtained with labeled compounds (previously mentioned) indicate that 1,1-dehydrogenation of the silyl group prevails. Thus, we conclude that the rate determining TS**2/14** en route to silylene formation is lower in energy than TS**8/10** (E_{rel} = 40.2 kcal/mol) and the entrance channel (E_{rel} = 37.8 kcal/mol).

5.3. Loss of methane

Only one pathway for the formation of **13** is calculated, e.g. primary C–C bond insertion, subsequent β-hydrogen migration from the silyl to the methyl group and final release of a methane molecule from **12** (Fig. 7). The reverse sequence, i.e. Si–H bond activation followed by a β-methyl migration is not pursued because previous studies have shown that migration of hydrogen is generally preferred over that of alkyl groups [66–68,93]. Compared to the other PES, the critical TS**11/12** (E_{rel} = 35.8 kcal/mol) is the lowest lying TS of all rate determining steps. The energetic location of TS**11/12** as well as the low-lying exit channel suggests C–C bond activation as the kinetically and thermodynamically most favored pathway for the reaction of **1** with Co^+. Notwithstanding, formation of CH_4 does not constitute the major route in the experimental studies.

Therefore, a closer inspection of the whole PESs (Figs. 4–7) is indicated. As the C(2)–H insertion pathway is less likely to occur due to the high energy demands of TS**4/7** and TS**7/8**, only the four remaining mechanisms have to be considered. The rate determining transition structures TS**3/4** (C–Si), TS**8/10** [C(1)–H], TS**11/12** (C–C), and TS**2/14** (Si–H) are located at E_{rel} = 39.6, 40.2, 35.8, and <40.2 kcal/mol, respectively; within the error bars of the calculations they are considered energetically comparable. Along these routes, all products are energetically located well below the corresponding TS; thus, based on these PESs a strong competition of these channels along with comparable branching ratios for the corresponding products is expected to occur. However, it is important to stress in this context, that even slight differences in the energetic location of the TS can cause the expected product branching ratios to change dramatically because of the exponential behavior of Arrhenius-type expressions; in addition, rate constants do not depend on activation energies alone.

Although, as mentioned above, the rate determining TS of several surfaces cannot be unequivocally assigned within the error of the method, our calculations show a strong trend towards formation of CH_4 as the kinetically and thermodynamically preferred neutral product; this contrasts with the experimental findings (Fig. 1). Several factors can be considered to explain this discrepancy. (1) Earlier calculations on the binding energies of M^+–CH_3 and $(H_3C)M^+$–CH_3 [94–96] and comparison with existing experimental data [97] (Table 1) show a distinct overestimation of the sum of the bond dissociation energies [$D_0(M^+$–$CH_3) + D_0(CH_3M^+$–$CH_3)$] in the B3LYP/BS1 approach for Fe^+. For Co^+, no experimental data are available, but comparison with ab initio calculations [96] (see Table 1) suggests a comparable effect. The $M(CH_3)_2^+$ species may be considered as a model system for a C–C inserted intermediate; therefore, a similar overestimation of M^+–C bond dissociation energies might effect the calculations of the C–C insertion. This would result in an artificial stabilization of **11** and TS**11/12** as compared to the corresponding structures of the Si–H and C–H insertion PESs, which is further supported by preliminary calculations on Co–CH_3, Co–SiH_3, and Co–H binding energies [98]. However, for the C–Si activation we would expect some overbinding as well. According to Table 1, we find the error due to this phenomenon amounts to 6.0 kcal/mol for $Fe(CH_3)_2^+$. If, as a rough first estimate, the same error is assumed for the C–C insertion PES in the present system, **11** and TS**11/12**

Table 1
Comparison of experimental, MCPF- and DFT-based bond dissociation energies (D_0) in kcal/mol of Co^+ and Fe^+ methyl and dimethyl complexes

	$D_{0,\text{ experimental}}$[a]	$D_{0,\text{ ab initio}}$[b]	$D_{0,\text{DFT}}$	$D_{0,\text{DFT}}$[e]
Fe^+–CH_3	54.6 ± 1.1	50.9	64.9[c]	60.9
H_3CFe^+–CH_3	43.1 ± 2.5	33.0		42.5
ΣD_0	97.7 ± 2.7	83.9		103.4
Co^+–CH_3	48.5 ± 0.9	48.6	56.3[d]	57.5
H_3CCo^+–CH_3		39.1		51.2
ΣD_0		87.7		108.7

[a] See [90].
[b] See [96].
[c] See [94].
[d] See [95].
[e] This work, obtained using the B3LYP/BS1 approach.

would have to be shifted to higher energies by some kilocalories per mole. This puts the C–C insertion PES into the same energy range as calculated for C–Si, C–H, and Si–H bond activations. Another hint that the C–C insertion may be artificially stabilized in the present computational approach arises from single-point calculations on the critical parts of the PES, i.e. the transition structures of the rearrangement and the exit channels, using a larger basis set (B3LYP/BS2, see Table 2). These calculations reveal small, but important changes in the qualitative picture as compared to the B3LYP/BS1 approach. Although the picture remains more or less unchanged for the product channels, small but crucial changes occur for the activation barriers. TS**11/12** of the C–C insertion PES corresponds in the B3LYP/BS2 picture no longer to the lowest transition state; rather this TS is located at the same relative energy as TS**8/10** and TS**3/4** within the error of the calculations, e.g. TS**11/12** is calculated 3.0 kcal/mol *above* TS**8/10** of the C(1)–H insertion PES and 3.0 kcal/mol below the corresponding TS of the C–Si insertion pathway (TS**3/4**). Thus, the B3LYP/BS2 results imply again that the different pathways strongly compete with each other under thermal conditions. Accordingly, the preference of C–C bond activation may no longer exist at higher levels of theory and may even disappear when higher levels of theory are used in geometry optimizations. It needs to be stressed again, however, that although distinction of the three TSs, which are explicitly discussed previously (TS**11/12**, TS**3/4**, and TS**8/10**), is not possible within the error of the calculations, differences of 3.0 kcal/mol (between TS**11/12** and TS**8/10** as well as between TS**3/4** and TS**11/12**) do matter in the experiment. The use of more sophisticated theoretical methods is therefore indicated and may be a possibility to distinguish more reliably between the different pathways. (2) The current calculations consist of purely stationary data. Introduction of dynamical features, for instance by doing RRKM calculations, may be necessary to describe the properties of the Co^+/ethylsilane system properly. Weisshaar et al. [78–80] have recently reported a qualitative description of the reactions of Ni^+ with propane and *n*-butane, by using B3LYP calculations, whereas quantitative modeling of the experimental data requires RRKM calculations and in particular the adjustment of the activation barriers predicted by the B3LYP calculations. Interestingly, each transition state leading to a different product has to be adjusted by a different energy, but all transition states are corrected in the same direction, i.e. to lower energies. The latter, as well as our own findings, seems to support the assumption of a general overestimation of barrier heights in the B3LYP approach. (3) Statistical arguments could also disfavor the formation of CH_4 in

Table 2
Calculated relative energies (kcal/mol) of the critical parts of the PES by using B3LYP/BS1, B3LYP/BS2, and B3LYP/BS1 under incorporation of thermal corrections[a]

	$E_{\text{rel,0 K}}$ (BS1/with ZPVE)	$E_{\text{rel,0 K}}$ (BS2/with ZPVE)[b]	$G_{298\text{ K}}$ (BS1)
Co^+ + **1**	37.8	41.7	30.2
TS**3/4**	39.6	40.7	39.0
TS**4/7**	44.6	46.3	44.3
TS**7/8**	46.0	46.4	46.2
TS**8/10**	40.2	34.7	41.2
TS**11/12**	35.8	37.7	34.7
5 + SiH_4	9.5	17.2	−0.7
9 + H_2	13.8	20.8	6.9
13 + CH_4	4.0	11.7	−6.4
14 + H_2	17.3	20.4	9.6

[a] All energies given refer to the lowest lying encounter complex **2** at $E_{\text{rel}} = 0$.
[b] As the B3LYP/BS2 calculations are only single point calculations, we used the ZPVEs computed with the B3LYP/BS1 approach.

the experiments. For instance, formation of product complex **5** can be achieved along two pathways [initial C–Si and C(2)–H bond insertion], both of which are feasible within the error of the calculations, although one of them is more likely to occur due to an energetically less demanding TS. Although the C–Si insertion pathway has only one possibility to evolve, C(2)–H insertion may occur at any of the three C–H bonds at C(2) atom, leaving us with a statistical weight of 3 for the C(2)–H insertion pathway and a statistical weight of 4 for both possible pathways the formation of **5**. A similar situation is found for the formation of the product complex **8**. Both pathways, C(1)–H and C(2)–H insertions are thermodynamically accessible, although C(1)–H insertion is favored because of the lower-lying TS. Although C(1)–H insertion has a statistical weight of 2 because insertion may occur into each of the two C–H bonds at C(1), the C(2)–H insertion pathway has a statistical weight of 3, as explained above. For the formation of **8** via both conceivable pathways this yields an overall statistical weight of 5. By using analogous arguments, loss of H_2 under formation of **15** is associated with a statistical weight of 3. In contrast, **12** can only be formed via a single pathway, and thus has a statistical weight of 1. Therefore, C–C bond cleavage is statistically disfavored compared to all other types of bond activation in the present system. (4) Finally, temperature effects need to be considered. The computational results presented up to this point always refer to 0 K energies. However, the internal temperature of the metastable Co^+/ethylsilane complexes examined in the sector-MS experiment is generally assumed to be 500 K, but higher values have also been reported before [28]. The internal temperature of the separated reactants in the FTICR experiments is assumed to be 298 K, and the internal energy content of the encounter complexes formed in the FTICR is expected to be much higher; as outlined above, the internal energy content of the encounter complexes in the FTICR is here even larger than in the sector-MS. Inclusion of thermal and entropic corrections in terms of relative ΔG_{298} values (Table 2) is therefore necessary but results in small changes of the picture in terms of absolute numbers only. Because the relative energies of both TS**11/12** and TS**3/4** decrease, the advantage of the C–C activation remains approximately the same indicating similar entropic effects. The disadvantage of the pathways based on initial C(2)–H bond insertion is still distinct, such that all deliberations lead to exclusion of this pathway from the expected course of the reaction. Obviously, however, thermal effects alone cannot account for the underestimation of the C–C bond activation pathway.

6. Summary

We have investigated the reactions of Co^+ with $C_2H_5SiH_3$ by using the DFT approach B3LYP with a basis set of VDZ-quality. First of all, the calculations show qualitative agreement with the experiments in that all products observed in the experiments are also calculated to be formed in reactions proceeding via exothermic or thermoneutral pathways. Although SiH_4 is easiest accessed via primary C–Si bond activation; the favored pathways for the formation of neutral H_2 are found to proceed via primary C(1)–H and Si–H insertion, respectively. Although C(2)–H insertion is also an approximately thermoneutral pathway within the error of the method of 8 kcal/mol, according to our calculations, it is less likely to occur due to the higher lying transition structures associated with the rearrangements along the initial C(2)–H insertion surface as compared to the existing alternatives on the C–Si, C(1)–H, C–C, and Si–H insertion PESs. For the formation of neutral CH_4 only one conceivable pathway is calculated, commencing with insertion in the C–C bond.

The quantitative consistency between experimental product branching ratios and calculations is less good. No clear-cut energetic distinction can be made between TS**3/4**, TS**8/10**, and TS**11/12** such that some disagreement between experiment and theory remains unresolved. Thus, the experimentally observed preference for loss of SiH_4 concomitant with formation of the charged product species **5** does not find a conclusive rationale in the theoretical predictions. Statistical factors and temperature effects are considered as explanations for this behavior but the major source of disagreement is attributed to the unbalanced descrip-

tion of M–H, M–C, and M–Si bond strengths in the investigated cationic complexes by the applied B3LYP functional in conjunction with the VDZ basis set.

An important conclusion derived from this study concerns the performance of currently used theoretical methods for the description of reactions involving transition-metal compounds. Thus, nowadays levels of theory are capable of describing the potential-energy surfaces involved in these processes qualitatively correct. In fact, the accuracy of the predicted barrier heights may even suffice for a quantitative assessment of branching ratios when *similar* processes compete with each other. For example, a combination of ab initio methods and molecular modeling proved successful in describing the regioselectivity in the remote functionalization of C–H bonds of nonanitrile/M^+ (M = Fe, Co) [28]. The agreement achieved between experiment and theory in this case is not considered as being entirely fortuitous because in the context of regioselectivity the pathways do not fundamentally differ in nature but in subtle effects imposed by the substrate's backbone. Therefore, the gross systematic error in describing certain bonding situations cancels in the evaluation of the branching for the activation of a certain site. In the present case, however, we compare channels which are *dissimilar* in that the nature of the bonds being activated differ, i.e. C–H, C–C, C–Si, and Si–H bonds. In such a case, even minute errors in quantitatively describing the bonding situations—recall the above discussion of the C–C insertion intermediates—results in dramatic changes of the predicted branching ratios. Thus, we conclude that the quantitative description of competing processes of different kind remains problematic. Moreover, for the time being it is doubtful that theory will reach the level of accuracy necessary to quantify branching ratios in competitive reactions of transition-metal mediated bond activations.

Acknowledgements

Financial support by the Deutsche Forschungsgemeinschaft, the Fonds der Chemischen Industrie, and the Volkswagen-Stiftung is gratefully acknowledged. The authors thank Dr. Georg Hornung and Dr. Ilona Kretzschmar for helpful discussions. Generous allocation of computer time by the Konrad-Zuse Zentrum für Informationstechnik Berlin is appreciated.

References

[1] A.E. Shilov, Activation of Saturated Hydrocarbons by Transition Metal Complexes, Reidel, Boston, MA, 1984.
[2] C.L. Hill, Activation and Functionalization of Alkanes, Wiley, New York, 1989.
[3] Selective Hydrocarbon Activation, J.A. Davies, P.L. Watson, J.F. Liebmann, A. Greenberg, (Eds.), VCH, Weinheim, 1990.
[4] D.H.R. Barton, Aldrichim. Acta 23 (1990) 3.
[5] R.H. Crabtree, Chem. Rev. 85 (1985) 245.
[6] K. Eller, H. Schwarz, Chem. Rev. 91 (1991) 1121.
[7] F. Garin, G. Maire, Acc. Chem. Res. 22 (1989) 100.
[8] K. Eller, Coord. Chem. Rev. 126 (1993) 93.
[9] B.S. Freiser, Acc. Chem. Res. 27 (1994) 353.
[10] B.A. Arndtsen, R.G. Bergmann, T.A. Mobley, T.H. Peterson, Acc. Chem. Res. 28 (1995) 154.
[11] R.H. Crabtree, Chem. Rev. 95 (1995) 987.
[12] A.E. Shilov, G.B. Shulpin, Chem. Rev. 97 (1997) 2879.
[13] B. Rybtchinski, D. Milstein, Angew. Chem. 38 (1999) 870.
[14] R. Breslow, Chem. Soc. Rev. 1 (1972) 553.
[15] R. Breslow, Acc. Chem. Res. 13 (1980) 170.
[16] R. Breslow, Acc. Chem. Res. 28 (1995) 146.
[17] H. Schwarz, Acc. Chem. Res. 22 (1989) 282.
[18] G. Czekay, T. Drewello, K. Eller, C.B. Lebrilla, T. Prüsse, C. Schulze, N. Steinrück, D. Sülzle, T. Weiske, H. Schwarz, in Organometallics in Organic Synthesis, H. Werner, G. Erker (Eds.) Springer, Heidelberg 1989, Vol. 2, p. 203.
[19] T. Prüsse, H. Schwarz, Organometallics 8 (1989) 2856.
[20] D. Schröder, H. Schwarz, J. Am. Chem. Soc. 112 (1990) 5947.
[21] T. Prüsse, J. Allison, H. Schwarz, Int. J. Mass Spectrom. Ion Processes 107 (1991) 553.
[22] T. Prüsse, A. Fiedler, H. Schwarz, Helv. Chim. Acta 74 (1991) 1127.
[23] D. Schröder, W. Zummack, H. Schwarz, J. Am. Chem. Soc. 116 (1994) 5857.
[24] G. Hornung, Ph.D. thesis, TU Berlin D83, 1998.
[25] T. Prüsse, Ph.D. thesis, TU Berlin D83, 1991.
[26] A. Hässelbarth, T. Prüsse, H. Schwarz, Chem. Ber. 123 (1990) 209.
[27] G. Hornung, D. Schröder, H. Schwarz, J. Am. Chem. Soc. 119 (1997) 2273.
[28] M.C. Holthausen, G. Hornung, D. Schröder, S. Sen, H. Schwarz, W. Koch, Organometallics 16 (1997) 3135.
[29] A. Hässelbarth, T. Prüsse, H. Schwarz, Chem. Ber. 123 (1990) 213.
[30] G. Hornung, S. Bärsch, D. Schröder, H. Schwarz, Organometallics 17 (1998) 2271.

[31] B.L. Kickel, P.B. Armentrout, J. Am. Chem. Soc. 117 (1995) 764.
[32] C.L. Haynes, Y.-M. Chen, P.B. Armentrout, J. Phys. Chem. 99 (1995) 9110.
[33] C.L. Haynes, Y.-M. Chen, P.B. Armentrout, J. Phys. Chem. 100 (1996) 111.
[34] K. Eller, H. Schwarz, Int. J. Mass Spectrom. Ion Processes 93 (1989) 243.
[35] K. Eller, W. Zummack, H. Schwarz, J. Am. Chem. Soc. 112 (1990) 621.
[36] R. Srinivas, D. Sülzle, T. Weiske, H. Schwarz, Int. J. Mass Spectrom. Ion Processes 107 (1991) 368.
[37] R. Srinivas, D. Sülzle, W. Koch, C.H. DePuy, H. Schwarz, J. Am. Chem. Soc. 113 (1991) 5970.
[38] C.A. Schalley, D. Schröder, H. Schwarz, Int. J. Mass Spectrom. Ion Processes 153 (1996) 173.
[39] C.A. Schalley, R. Wesendrup, D. Schröder, T. Weiske, H. Schwarz, J. Am. Chem. Soc. 117 (1995) 7711.
[40] D. Schröder, H. Schwarz, J. Organomet. Chem. 504 (1995) 123.
[41] G. Hornung, S. Bärsch, H. Schwarz, unpublished.
[42] M.R. Sievers, L.M. Jarvis, P.B. Armentrout, J. Am. Chem. Soc. 120 (1998) 1891.
[43] M.J. Frisch, G.W. Trucks, H.B. Schlegel, P.M.W. Gill, B.G. Johnson, M.A. Robb, J.R. Cheeseman, T.A. Keith, G.A. Petersson, J.A. Montgomery, K. Raghavachari, M.A. Al-Laham, V.G. Zakrzewski, J.V. Ortiz, J.B. Foresman, J. Cioslowski, B.B. Stefanov, A. Nanayakkara, M. Challacombe, C.Y. Peng, P.Y. Ayala, W. Chen, M.W. Wong, J.L. Andres, E.S. Replogle, R. Gomperts, R.L. Martin, D.J. Fox, J.S. Binkley, D.J. Defrees, J. Baker, J.P. Stewart, M. Head-Gordon, C. Gonzalez, J.A. Pople, GAUSSIAN 94, Revision A.1, Gaussian Inc., Pittsburgh, PA, 1995.
[44] C. Lee, W. Yang, R.G. Parr, Phys. Rev. B 37 (1988) 785.
[45] A.D. Becke, J. Chem. Phys. 98 (1993) 5648.
[46] E. Folga, T. Ziegler, Can. J. Chem. 70 (1992) 333.
[47] R.H. Hertwig, K. Seemeyer, H. Schwarz, W. Koch, Chem. Eur. J. 3 (1997) 1315.
[48] N. Sändig, W. Koch, Organometallics 16 (1997) 5244.
[49] A. Schafer, H. Horn, R. Ahlrichs, J. Chem. Phys. 97 (1992) 2571.
[50] "Standard" refers to the default setting in GAUSSIAN 94: Max. force = 0.000 45; rms force = 0.000 30; Max. displacement = 0.001 80; rms displacement = 0.001 20.
[51] K. Fukui, J. Phys. Chem. 74 (1970) 4161.
[52] C. Gonzales, H.B. Schlegel, J. Chem. Phys. 90 (1989) 2154.
[53] A.J.H. Wachters, IBM Tech. Rep. RJ584, 1969.
[54] A.J.H. Wachters, J. Chem. Phys. 52 (1970) 1033.
[55] f exponents are taken from: C.W. Bauschlicher, S.R. Langhoff, L.A. Barnes, J. Chem. Phys. 91 (1989) 2399.
[56] T.H. Dunning Jr., J. Chem. Phys. 90 (1989) 1007.
[57] R.A. Kendall, T.H. Dunning, R.J. Harrison, J. Chem. Phys. 96 (1992) 6796.
[58] D.E. Woon, T.H. Dunning, J. Chem. Phys. 98 (1993) 1358.
[59] C.E. Moore, Atomic Energy Levels, National Standards Ref. Data; National Bureau of Standards NSRDS-NBS 35, Washington, DC, 1971.
[60] M. Hendrickx, M. Ceulemans, L. Vanquickenborne, Chem. Phys. Lett. 254 (1996) 307.
[61] O. Gunnarson, R.O. Jones, Phys. Rev. B 31 (1985) 7588.
[62] T. Ziegler, J. Li, Can. J. Chem. 72 (1994) 783.
[63] T.V. Russo, R.L. Martin, P.J. Hay, J. Chem. Phys. 101 (1994) 7729.
[64] E.J. Baehrends, V. Branchadell, M. Sodupe, Chem. Phys. Lett. 265 (1997) 481.
[65] The reactions employed in this procedure are: (a) $CoCH_3^+ \rightarrow Co^+ + CH_3$, (b) $2CH_4 \rightarrow C_2H_4 + 2H_2$, and (c) $CoC_2H_4^+ \rightarrow Co^+ + C_2H_4$.
[66] M.C. Holthausen, A. Fiedler, H. Schwarz, W. Koch, Angew. Chem. 107 (1995) 2430.
[67] M.C. Holthausen, W. Koch, Helv. Chim. Acta 79 (1996) 1939.
[68] M.C. Holthausen, A. Fiedler, H. Schwarz, W. Koch, J. Phys. Chem. 100 (1996) 6236.
[69] M. Brookhart, M.L.H. Green, L.-T. Wong, Prog. Inorg. Chem. 36 (1988) 1.
[70] O. Eisenstein, Y. Jean, J. Am. Chem. Soc. 107 (1985) 1177.
[71] For an example of a combined theoretical and experimental study on the activation of SiH_4 with tungsten cations, see: A. Ferhati, T.B. McMahon, G. Ohanessian, J. Am. Chem. Soc. 118 (1996) 5997. Note, though, that the computational efforts do not include treatment of the full PES but rather concentrate on the structural assignment of experimentally observed products.
[72] For an example of an existing Si–H inserted structure, see: D.G. Musaev, K. Morokuma, J. Am. Chem. Soc. 117 (1995) 799. Note, however, that the existence of the Si–H inserted structure may be attributed to the steric crowding in the activating Rh(Cp)(CO) complex, which prevents formation of the sterically demanding four-centered transition state.
[73] D.G. Musaev, K. Morokuma, J. Phys. Chem. 100 (1996) 11600.
[74] D.G. Musaev, K. Morokuma, J. Chem. Phys. 101 (1994) 10697.
[75] D.G. Musaev, K. Morokuma, N. Koga, K.A. Nguyen, M.S. Gordon, T.R. Cundari, J. Phys. Chem. 97 (1993) 11435.
[76] T.A. Halgreen, W.N. Lipscomb, Chem. Phys. Lett. 49 (1977) 225.
[77] C. Peng, H.B. Schlegel, Israel J. Chem. 33 (1993) 449.
[78] R.J. Noll, S.S. Yi, J.C. Weisshaar, J. Phys. Chem. A 102 (1998) 386.
[79] S.S. Yi, M. Blomberg, P.E.M. Siegbahn, J.C. Weisshaar, J. Phys. Chem. A 102 (1998) 395.
[80] M. Blomberg, S.S. Yi, R.J. Noll, J.C. Weisshaar, J. Phys. Chem. A 103 (1999) 7254.
[81] D.B. Jacobson, R. Bakhtiar, J. Am. Chem. Soc. 115 (1993) 10830.
[82] R. Bakhtiar, C.M. Holznagel, D.B. Jacobson, J. Am. Chem. Soc. 115 (1993) 345.
[83] H. Kang, D.B. Jacobson, S.K. Shin, J.L. Beauchamp, M.T. Bowers, J. Am. Chem. Soc. 108 (1986) 5668.
[84] R. Probst, C. Leis, S. Gampers, W.E. Herdweck, C. Zybill, N. Auner, Angew. Chem. 30 (1991) 1132.
[85] D.A. Straus, C. Zhang, N. Quimbita, S.D. Grumbine, R.H.

Heyn, T.D. Tilley, A.L. Rheingold, S.J. Geib, J. Am. Chem. Soc. 112 (1990) 2673.
[86] H. Tobita, K. Ueno, M. Shimoi, H. Ogino, J. Am. Chem. Soc. 112 (1990) 3415.
[87] A. Jutzi, A. Mohrke, Angew. Chem. 29 (1990) 893.
[88] L.J. Procopio, D.H. Berry, J. Am. Chem. Soc. 113 (1991) 4039.
[89] T.S. Koloski, P.J. Carroll, D.H. Berry, J. Am. Chem. Soc. 112 (1990) 6405.
[90] B.K. Campion, R.H. Heyn, T.D. Tilley, J. Am. Chem. Soc. 112 (1990) 4079.
[91] D.H. Berry, L.J. Procopio, J. Am. Chem. Soc. 111 (1989) 4099.
[92] B.K. Campion, R.H. Heyn, T.D. Tilley, J. Am. Chem. Soc. 110 (1988) 7558.
[93] Note, however, that CH_3 migration is not impossible; for an example, see: S. Karraß, H. Schwarz, Organometallics 9 (1990) 2409.
[94] M.C. Holthausen, C. Heinemann, H.H. Cornehl, H. Schwarz, W. Koch, J. Chem. Phys. 102 (1995) 4931.
[95] M.C. Holthausen, Ph.D. Thesis, TU Berlin D83, 1996.
[96] M. Rosi, C.W. Bauschlicher, S.R. Langhoff, H. Partridge, J. Chem. Phys. 94 (1990) 8685.
[97] P.B. Armentrout, B.L. Kickel, in Organometallic Ion Chemistry, B.S. Freiser (Ed.), Kluwer Academic, Dordrecht, 1996.
[98] S. Bärsch, H. Schwarz, unpublished work. Note that all experimental data are taken from [94]; Co–H^+: D_0 = 45.7 ± 1.4 kcal/mol (expt.) and 34.7 kcal/mol (B3LYP/VDZ), Co–CH_3^+: D_0 = 48.5 ± 0.9 kcal/mol (expt.) and 57.5 kcal/mol (B3LYP/VDZ), Co–SiH_3^+: D_0 = 45.2 ± 3.0 kcal/mol (expt.) and 54.0 kcal/mol (B3LYP/VDZ).